Inorganica Chimica Acta 506 (2020) 119552

Contents lists available at ScienceDirect

Inorganica Chimica Acta

journal homepage: www.elsevier.com/locate/ica

Research paper

Evaluating the involvement of tryptophan on thiolated peptide-mercury(II) complexes: Cation-pi interactions

Maria Ngu-Schwemlein*, John Merle, William Meeker, Kierah Risdon-Langdon, Timothy Nixon

Department of Chemistry, Winston-Salem State University, Winston Salem, NC 27110, USA

ARTICLE INFO

Keywords:
Mercury(II)-peptide complexes
Cation-pi interaction
Metal-ligand charge transfer
Circular dichroism
Computational modeling

ABSTRACT

An understanding of how mercury(II) forms complexes with bis-cysteinyl peptides containing auxiliary binding groups could provide vital insights for optimal mercury immobilization. In this study, we investigate how tryptophan might participate in peptide-mercury(II) complex formation. Model pentapeptides consisting of a Cys-Xaa-Cys (CXC) sequence, where Xaa is Gly (**Penta 1**), Trp (**Penta 2**), and D-Trp (**Penta 3**) were designed. Their complexation with mercury(II) was studied by spectroscopic methods and molecular modeling. UV absorption difference spectra reflect the formation of bisthiolate-mercury(II) bonds. These spectra also show changes in the B_b absorption band of the indole group following complex formation. Circular Dichroism (CD) spectra indicate that mercury(II) bound peptides adopt a secondary structure resembling a type I β turn structure. Mercury(II) bound **Penta 2** also develops a negative CD band at 221 nm, which suggests an association between the tryptophan indole ring and mercury(II) via cation-pi interaction. Fluorescence quenching in the presence of equimolar mercury(II) is significantly greater for **Penta 2** than **Penta 3**. These CD and fluorescence data indicate that the indole ring of **Penta 3** is not interacting with the coordinated mercury(II). Optimized 1:1 mercury(II)-peptide structures show that the indole pi system of **Penta 2** participates in mercury(II) cation-pi interaction, whereas in **Penta 3** it is involved in ammonium cation-pi association. These structural insights will be useful for designing more effective mercury chelators containing tryptophan as an auxiliary binding and hydrophobic shielding group in immobilizing mercury(II).

1. Introduction

Bis-cysteinyl sequences are present in many metal binding and transport proteins. The two-cysteine residues of Cys-Xaa-Cys (CXC) and CXXC motifs are found in various types of metal-binding proteins such as metallothioneins, ferrodoxins, bacterial mercury detoxification systems, MerP and MerA [1–3], and in copper chaperone proteins HAH1 and CopZ [4,5]. Coordination to cysteine residues dominates in these metal-protein associations. Small peptide models containing such motifs have been designed to find effective heavy metal-coordinating ligands [6–8]. Although thiols are usually the primary ligating points in such metal ion coordination, various other functional groups in peptides (amide, N-terminal ammonium, C-terminal carboxylate, and side chain groups) could participate in auxiliary metal ion complex stabilization. Kinetically inert mercury(II) complexes could be very useful as chelating agents for the elimination of toxic metal ions from humans, or contaminated wastewater. An understanding of how mercury ions form complexes with thiolated peptides, which contain specific auxiliary binding group(s), could provide useful insights for optimal mercury immobilization.

Cation-pi interactions between the indole side chain of tryptophan residues in proteins is increasingly recognized as an important electrostatic interaction that provides distinct contributions toward the formation and functioning of some proteins and metalloproteins [9–13]. This noncovalent interaction type involves the electron rich cloud of aromatic pi electrons and a positively charged cation, among them metal cations like Cu^{2+} and Ni^{+}, and cationic amines like arginine and histidine [14–17]. Metal ions also have a tendency to bind at centers of high hydrophobicity contrast in proteins. This qualitative feature was found at the binding site of various metalloproteins and was therefore proposed as an environment required for metal binding and can be used in de novo design to increase metal ion affinity for a binding site [18]. Studies by others also show that assembling of amino acid side chains close to the metal coordination site can stabilize a metal complex by creating a hydrophobic fence that can shield the coordinated metal from attack by other competing ligands [14,19]. Another recent investigation of the crystal structures of metalloproteins in the Protein Data Bank also revealed that aromatic residues such as

* Corresponding author at: 601 M.L. King Jr. Drive, W.B. Atkinson Science Bldg., Winston-Salem, NC 27110, USA.
E-mail address: Schwemleinmn@wssu.edu (M. Ngu-Schwemlein).

https://doi.org/10.1016/j.ica.2020.119552
Received 22 January 2020; Received in revised form 22 February 2020; Accepted 23 February 2020
Available online 25 February 2020

tryptophan situated close to a metal ion center interact with the coordinated ligands [20]. All these studies indicate that the side chain group of tryptophan could be a promising auxiliary binding group to stabilize the mercury(II) complex via cation-pi interaction or by creating a hydrophobic barrier that could shield the coordinated mercury ion from undergoing ligand exchange.

Recently, we reported how an added gamma carboxylate group in a tripeptide ligand, Cys-Glu-Cys (CEC), affects mercury complex formation, speciation trends, and their relative stabilities [21]. In building upon this work, the aim of this study is to gain an understanding of how a tryptophan residue in a CXC motif might participate in complex formation involving mercury(II). In this study, a simple model pentapeptide Gly-Cys-Gly-Cys-Gly (**Penta 1**) was selected for investigating its mercury(II)-sulfur coordination preferences and its peptide backbone turn tendency upon mercury(II) binding. With the aim to investigate the possible involvement of tryptophan in auxiliary binding, **Penta 2** (Gly-Cys-Trp-Cys-Gly) was designed. **Penta 3** (Gly-Cys-D-Trp-Cys-Gly) was included in this comparative study to evaluate the effect of reversing the stereochemical configuration of tryptophan. Here we present some spectroscopic characterization of the mercury(II) binding properties of these pentapeptides. The structures of the 1:1 mercury(II) complex for each pentapeptide were also optimized to understand how the indole group could be involved in complex formation. These structural insights will be useful for the rational design of mercury chelators, and in understanding how mercury(II) may form complexes with some endogenous metalloproteins.

2. Experimental

2.1. Materials

Mercury(II) chloride (> 99.5%) was obtained from Millipore-Sigma (St. Louis, Missouri, USA). HPLC grade acetonitrile and water, high purity sodium hydrogen phosphate and sodium dihydrogen phosphate, Durapure 0.22 μm filters, and HPLC grade water were purchased from Fisher Scientific (Pittsburgh, Pennsylvania, USA). Custom designed pentapeptide models, **Penta 1**, **2**, **and 3**, were purchased from Genscript (Piscataway, New Jersey, USA) at > 98% purity. **Penta 1** (ESI-MS $[M + H]^+$ is 396.1, peptide content = 77.6%), **Penta 2** ESI-MS $[M + H]^+$ is 525.1, peptide content = 73.3%), and **Penta 3** (ESI-MS $[M + H]^+$ is 525.1, peptide content = 79.9%). The concentration of **Penta 1** solutions was also confirmed by its UV absorbance, **Penta 1** (ε_{214nm} = 4205 M^{-1} cm^{-1}) [22]. The UV absorption intensity of Trp (ε_{280nm} = 5500 M^{-1} cm^{-1}) was used for determining the peptide solution concentrations of **Penta 2** and **Penta 3**.

2.2. UV–vis spectroscopy

Reaction mixtures of the pentapeptides titrated with $HgCl_2$ in 50 mM sodium phosphate, pH 6.6 were studied by UV–vis spectroscopy on a dual beam Shimadzu UV-2401PC series UV–vis spectrophotometer. UV absorption spectra were acquired at room temperature using a 1 cm path-length quartz cuvette. A 2.5 mL solution consisting of 100 μM peptide in 50 mM phosphate pH 6.6 buffer was titrated with aliquots of a 50 mM $HgCl_2$ stock solution. For each $HgCl_2$ addition, an equivalent addition was made in the reference cell containing only 50 mM sodium phosphate buffer pH 6.6, so that the absorption difference spectrum can be attributed to the binding of Hg^{2+} to the peptide. The reaction mixture was mixed and stirred for 1 min followed by an additional 2 min equilibration. The ligand metal charge transfer (LCMT) band for the binding of Hg^{2+} to the thiolates was monitored between 200 and 350 nm. The UV spectrum arising from the binding of the Hg^{2+} to peptide was obtained by subtracting the background of the peptide in the absence of Hg^{2+}. Caution: Mercury compounds are hazardous and should be handled with proper precautions, and they must be disposed in chemical waste containers designated for heavy metals.

2.3. Circular dichroism

CD spectroscopic measurements were conducted on a Jasco J-815 Circular Dichroism Spectrometer (Easton, Maryland, USA) equipped with a Peltier temperature controlled cell holder (PTC-423S/C). Spectra were recorded at 25°C using a 0.1 cm path-length quartz cell with the following parameters: standard sensitivity = 100 mdeg; continuous scanning mode at 50 or 100 nm/min; bandwidth = 1.0 nm; response = 4 *sec*; data pitch = 0.1 nm. Peptide solutions were prepared at 100 μM in 50 mM sodium phosphate, pH 6.6. Each spectrum represents an average of four consecutive scans. The mercury(II) binding reaction mixture was prepared by titrating an aliquot of a 100 mM $HgCl_2$ stock solution into the respective peptide solution. Molar ellipticity (ME, in deg M^{-1} cm^{-1}) was determined using the spectral analysis platform in the Jasco Spectra Manager™ version 2 program (Jasco software, Inc.), where molar ellipticity (ME) = $100\theta/(Cl)$, θ is the degree of ellipticity, C is the molar concentration of the peptide, and l is the cell path in cm.

2.4. Fluorescence

Fluorescence spectroscopy measurements were carried out on a FluoroMax spectrofluorimeter (Horiba Scientific, New Jersey, USA), equipped with a Peltier temperature controlled cell holder (SGL-POS QNW W/CIR). The fluorescence emission spectra were recorded using 10 μM peptide solutions in a 3 mL quartz cell with a path length of 1 cm. Mercury chloride stock solution was prepared at 5 mM and added to the peptide in 50 mM sodium phosphate buffer, pH 6.6. The reaction mixture was equilibrated for 5 min before its fluorescence spectrum was acquired. The excitation wavelength was set at 280 nm with a slit width of 3 or 4 nm. The emission spectra were recorded between 295 and 500 nm with the emission slit fixed at 3 or 4 nm. The dependency of the fluorescence intensity on quencher concentration was studied by the Stern–Volmer equation: $F_0/F = 1 + K_{SV}[Q]$, where F_0 and F are the fluorescence intensities in the absence and presence of the quencher, respectively. K_{SV} is the Stern–Volmer constant, and [Q] is the concentration of the quencher [23]. Variable temperature Stern–Volmer plots were conducted at 25°C, 35°C, and 45°C.

2.5. Computational methods

Low energy conformations for **Penta 1**, **Penta 2** and **Penta 3** complexes were sought using the Systematic Pseudo Monte Carlo Multiple Minimum (SPMC) search method implemented in Macromodel with each accepted structure being geometry optimized [24]. The OPLS2005 molecular mechanics force field was used for energy evaluations and geometry optimizations with solvent excluded. The OPLS2005 force field does not include parameters for Hg^{2+} so Sr^{2+} was inserted in place of mercury (II) due to size and charge similarities. The force field generated geometry about strontium (II) is the same basic geometry about mercury (II) for the complexes studied. After conformational searching, mercury (II) was used on all subsequent calculation. For each complex, 500,000 conformations were generated and the 1000 lowest energy structures were saved. All 1000 structures underwent single-point energy evaluations using the M06-2X density functional theory (DFT) method with LANL2DZ basis set and effective core potential (ECP) under vacuum conditions. The 150 most stable complex geometries were optimized using the M06-2X DFT method combined with 6-31G(d,p) basis set on non-metal atoms and Stuttgart/Dresden (SDD) basis set with pseudo-potential for 60 core electrons on mercury atom [25]. The M06-2X functional has been applied previously to obtain quality geometries for peptides and Hg(II)-peptide complexes [21,26,27]. Vibrational frequencies were calculated for all optimized geometries to ensure no imaginary vibrational frequencies. M06-2X geometry optimizations and vibrational frequency calculations were performed with the Polarizable Continuum Model (PCM) using the

integral equation formalism variant (IEFPCM) (SMD) solvation model with water as solvent [28]. The van der Waals sphere size for mercury was set to 2.34 Å as previously described [27].

To estimate the stability of each complex structure the Gibbs energy in solution (G_{soln}) for each was calculated by summing the gas phase Gibbs energy (G_{gas}) and Gibbs energy of solvation (ΔG_{solv}).

$$G_{soln} = G_{gas} + \Delta G_{solv}$$

To obtain the gas phase Gibbs energy (G_{gas}), structures were energy evaluated in vacuum with the Moller-Plesset second-order perturbation theory method with all excitations included (MP2(full)) combined with a 6-311G(d, p) basis set on non-metal atoms and cc-pVDZ-PP basis set and ECP on mercury. Our previous studies, have shown this method to give energies for mercury-thiol complexes in good agreement with CCSD(T)/CBS(2,3) values [27]. Thermal corrections to 298.15 K at 1 atm were determined using the M06-2X solution phase vibrational frequency calculations. While these are not gas phase thermal corrections, it has been shown that the use of solution phase corrections introduce negligible error [29]. Solution phase geometry optimizations were required to maintain a zwitterion protonation state for complexes. The M06-2X/6-31G(d,p)/SDD zero-point vibrational energies were scaled by 0.950 [30]. The Gibbs energy of solvation (ΔG_{solv}) was determined using the SMD model with water solvent by performing a self-consistent PCM calculation using the M06-2X/6-31G(d,p)/SDD method using all default van der Waals sphere sizes. The energy to compress to gas from and ideal gas (1 mol/22.4 L) to 1 M was not factored in since the goal was to identify the complexes with lowest Gibbs energy in solution. The Gaussian09 software was used for all M06-2X and MP2 calculations [31].

3. Results

3.1. UV–vis absorption spectrometry

Complex formation between mercury(II) and the pentapeptides was studied by monitoring the ligand-to-metal charge-transfer (LMCT) transitions within the UV energy range. Fig. 1 shows the absorption difference spectra for the titration of mercury(II) into a solution of **Penta 1**. These difference spectra were obtained by subtracting the UV absorption contributed by **Penta 1** in the absence of mercury(II). Titration of mercury(II) into **Penta 1** results in increase of extinction coefficients at ca. 210 nm and 220 nm up to 1.0 equiv of mercury(II) to **Penta 1**. The observed ~210 nm absorption difference band reflects changes in the peptide backbone amide absorption (n to π*) when **Penta 1** interacts with mercury(II). The ~220 nm absorption shoulder band shows a mercury(II) concentration dependent increase indicating the formation of mercury(II)-peptide complex, with an extinction coefficient of 10380 $M^{-1}cm^{-1}$ at 1:1 mercury(II): **Penta 1** stoichiometry (Fig. 1 inset). This is similar to those observed for linear, bis-thiolated mercury complexes, where two thiolate-coordinated mercury complexes have been shown to exhibit a characteristic high-energy LMCT band below 250 nm [6,8]. However, in excess of mercury(II), the rate of change in extinction coefficient at 220 nm decreases (Fig. 1 inset), accompanied by a concomitant small increase in absorbance at 260 nm (Fig. S1). These new transitions may indicate the formation of polymetallic mercury species as previously reported by others [6]. Trigonal thiolated mercury(II) complexes [$Hg(SR)_3$] and tetrahedral Hg $(SR)_4$ species have been shown to exhibit lower energy LMCT band around 240–300 nm compared to linear bisthiolated mercury complexes [32–35].

Titration of mercury(II) to **Penta 2** yielded absorption difference spectra consisting of two absorbance maxima at ~210 nm and ~227 nm (Fig. 2). The ~210 nm absorbance band is similar to that exhibited by **Penta 1** and reflects changes in the peptide amide absorption when it complexes mercury(II). However, the ~220 nm absorbance shoulder in **Penta 1** is replaced by an absorbance maximum band at ~227 nm. Following titrations of **Penta 2** with increasing equiv of mercury(II), this 227 nm band becomes better defined (Fig. 2). This could be due to contributions from changes in the strong B_b absorption of the indole ring in **Penta 2** upon complex formation. Similar to **Penta 1**, the increase in extinction coefficient at 227 nm also exhibits a linear dependency on the concentration of mercury(II) (Fig. 2 inset). In excess of mercury(II), some insoluble polymetallic mercury species were formed.

Fig. 3 shows the corresponding absorption difference spectra for **Penta 3**. Two absorbance maxima are also observed at ~210 nm and ~226 nm. The ~226 nm absorbance band could also be attributed to contributions from the LMCT transition band for Hg-S bonds and changes in the B_b absorption of the indole ring when **Penta 3** binds mercury(II). It also shows changes in extinction coefficient values that is linearly dependent on mercury(II) concentration (Fig. 3 inset).

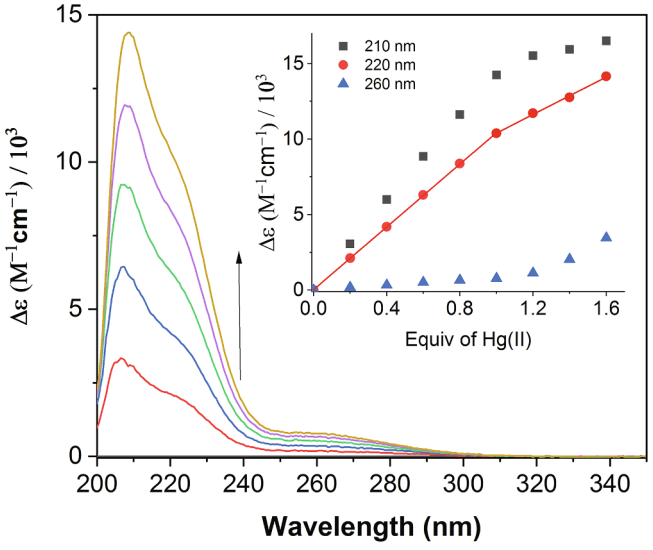

Fig. 1. UV absorption difference spectra [Δε = ε(HgPenta1) - ε(Penta1)] correspond to **Penta 1** titrated with increasing mole equiv of $HgCl_2$. Inset shows changes in extinction coefficient values at 210, 220, and 260 nm versus mole equiv of $HgCl_2$ added.

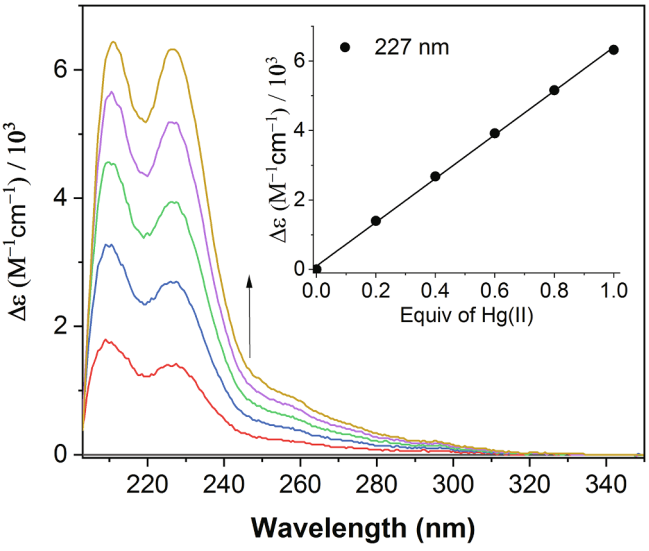

Fig. 2. UV absorption difference spectra [Δε = ε(HgPenta2) - ε(Penta2)] correspond to **Penta 2** titrated with increasing mole equiv of $HgCl_2$. Inset shows the change in extinction coefficient value at 227 nm versus mole equiv of $HgCl_2$ added.

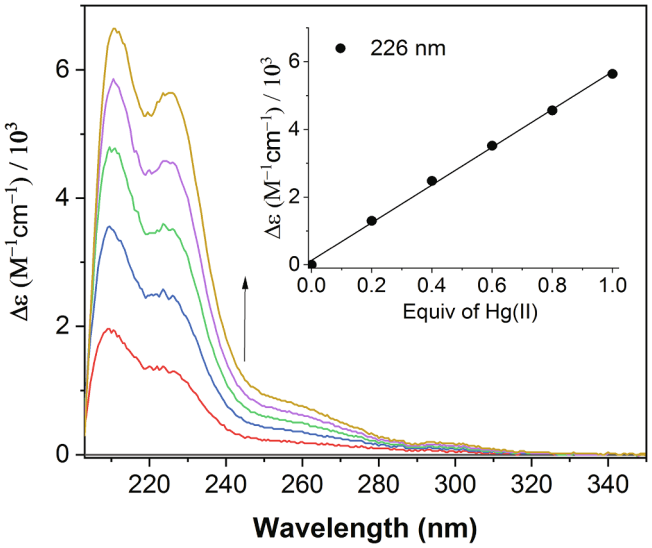

Fig. 3. UV absorption difference spectra [Δε = ε(HgPenta3) - ε(Penta3)] correspond to **Penta 3** titrated with increasing mole equiv of $HgCl_2$. Inset shows the change in extinction coefficient value at 226 nm versus mole equiv of $HgCl_2$ added.

3.2. Structural studies by circular dichroism

The secondary structural changes in these peptides on interaction with mercury(II) were studied by Circular Dichroism (CD) spectroscopy. Fig. 4 shows the CD spectra of **Penta 1** following titrations with mercury(II). **Penta 1** exhibits very little secondary structure as reflected by its weak CD spectrum. On binding mercury(II), it shows a CD spectrum resembling a type I β turn, which reverses the peptide chain direction, reminiscent of a class B CD spectrum [strong positive band between 200 and 210 nm (nπ* transition), and a strong negative band predicted between 180 and 190 nm (ππ* transitions)] [36]. As shown in Fig. 4 inset, the addition of mercury(II) resulted in an increase in the positive ellipticity at 208 nm and a corresponding increase in the negative ellipticity at 193 nm. These spectra also exhibit one isodichroic point at 198 nm suggesting transitions to a unique secondary structural 1:1 mercury(II):**Penta1** species. In excess of mercury(II), the magnitudes of the ellipticities at 208 nm and 193 nm decrease

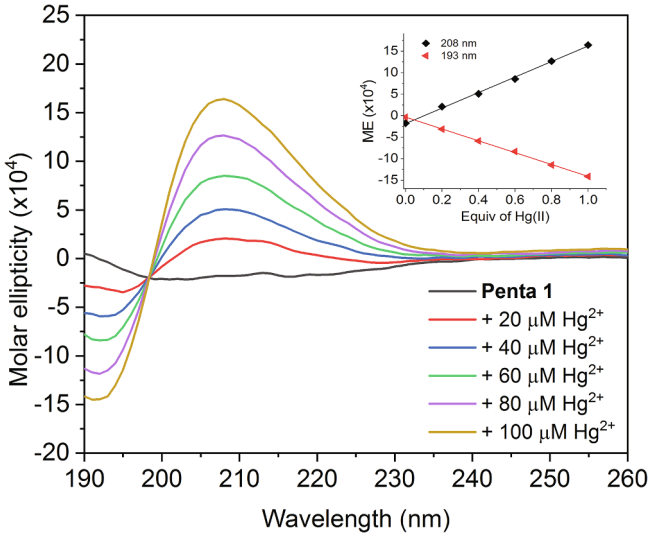

Fig. 4. Circular dichroism spectra of **Penta 1** following titrations with increasing mole equiv of $HgCl_2$. Inset shows the change in molar ellipticity value at 193 nm and 208 nm versus mole equiv of $HgCl_2$ added.

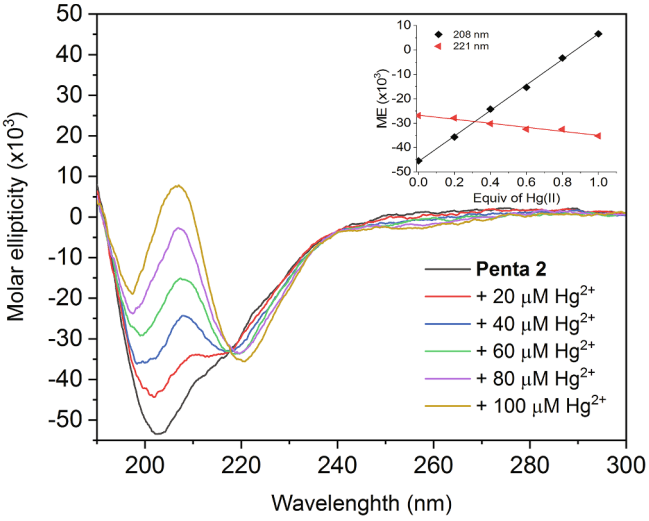

Fig. 5. Circular dichroism spectra of **Penta 2** following titrations with increasing mole equiv of $HgCl_2$. Inset shows the change in molar ellipticity value at 208 nm and 221 nm versus mole equiv of $HgCl_2$ added.

correspondingly. This may indicate the formation of polymetallic species with loss of structural integrity.

On titration of mercury(II) into **Penta 2**, the negative band at 202 nm decreases in intensity and gradually undergoes a blue-shift to 197 nm at 1:1 stoichiometric ratio of mercury(II) to **Penta 2**. Concomitantly, a positive CD band at 208 nm forms, accompanied by a negative band at 221 nm (Fig. 5 and inset). Additionally, these spectra share a common isodichroic point at 218 nm, suggesting structural transitions toward a well-defined secondary structure. In the presence of equimolar mercury(II), both **Penta 1** and **Penta 2** show a negative band below 200 nm and a positive band at 208 nm. However, the intensity of these bands for **Penta 2** are much weaker. More significantly, a newly formed strong negative band at ~221 nm dominates the CD spectrum of **Penta 2** in equimolar mercury(II). This band could be attributed to an interaction between the aromatic indole pi system and mercury(II). Takeuchi et al previously reported a similar development of a negative CD band at 223 nm, which was characterized as a signature CD band for a Cu^{2+}-Trp cation-pi interaction [37]. In the near-UV (260–320 nm) region of the CD, these spectra do not exhibit any strong CD signal indicating that there is no oxidation of Cys during the addition of mercury(II). Disulfide bond formation would generate a nσ* S—S transition band.

The CD spectrum of the free **Penta 3** (Fig. 6) is characteristic of a type II β turn structure, which is α-helix-like. It exhibits a negative band at 222 nm due to the peptide nπ* transition, and the negative 208 nm and positive 192 nm bands of the peptide ππ* transition [38]. Titration of mercury(II) to it resulted in the formation of a positive band at 208 nm and a negative band at 193 nm, accompanied by a gradual red-shift and weakening of the 222 nm peptide nπ* transition (Fig. 6 and inset). At 1:1 stoichiometric ratio of mercury(II) to **Penta 3**, the resulting CD spectrum resembles that for the corresponding **Penta 1** (Fig. 4). Similarly, an isodichroic point is observed for these spectra, suggesting a two-state structural transition between the unbound and mercury(II) bound **Penta 3**.

3.3. Tryptophan fluorescence spectroscopy

Tryptophan fluorescence is highly sensitive to its environment, including changes in polarity, and non-covalent interactions such as pi-cation associations involving metal or ammonium ions [10,13,39–41]. Its fluorescence emission is sensitive to quenching by mercury(II) through molecular contact. This can be due to complex formation, which is static quenching, or due to diffusive encounters, which is

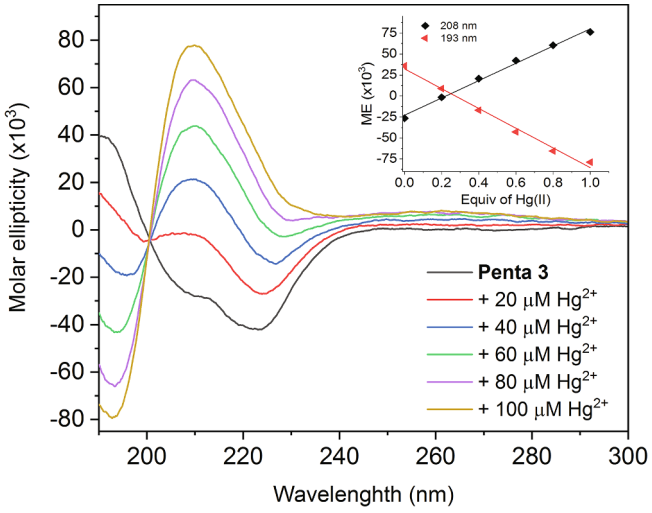

Fig. 6. Circular dichroism spectra of **Penta 3** following titrations with increasing mole equiv of $HgCl_2$. Inset shows the change in molar ellipticity value at 193 nm and 208 nm versus mole equiv of $HgCl_2$ added.

dynamic quenching [23]. They can be distinguished by their different dependency on temperature. Dynamic quenching is a diffusion-controlled process, which increases at higher temperature due to faster diffusion. On the other hand, higher temperature usually decreases static quenching due to dissociation of weakly bound complexes [23]. Therefore, quenching measurements can be used to reveal the type of interaction between the indole ring and mercury(II).

Fig. 7 shows the fluorescence emission spectra of **Penta 2** following titrations with mercury(II) at 25°C. At equimolar ratio of mercury(II) to **Penta 2**, about 70% of its intrinsic fluorescence is quenched. Fig. 7 (inset) presents the Stern-Volmer plot for the quenching of tryptophan emission by mercury(II) at three different temperatures (25°C, 35°C, and 45°C). They reveal quenching effects in which F_0/F is dependent upon the concentration of mercury(II). These Stern-Volmer plots show an upward curvature reflecting both static and dynamic quenching for the tryptophan fluorescence. However, they do not change significantly when the temperature was raised from 25°C to 45°C, suggesting that the contribution from static quenching is larger than dynamic or collisional quenching in this temperature range. These quenching effects are indicative of molecular contact between the indole ring and mercury(II).

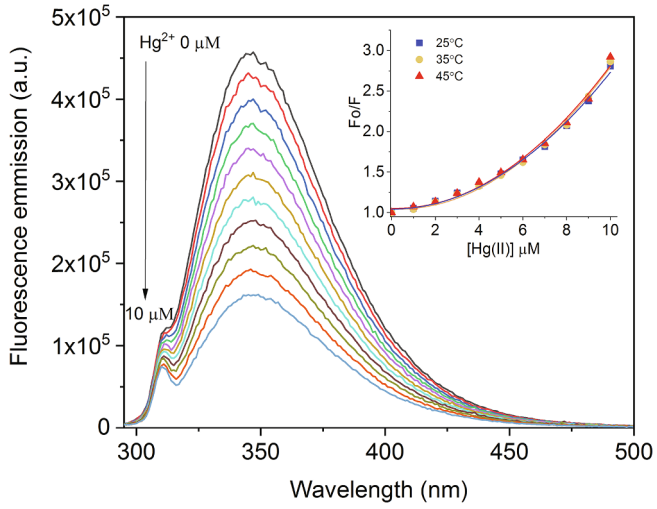

Fig. 7. Fluorescence spectra of 10 μM **Penta 2** following titration with increasing concentrations of mercury(II) at 20°C. Inset: Stern-Volmer plots at 25°C, 35°C, and 45°C.

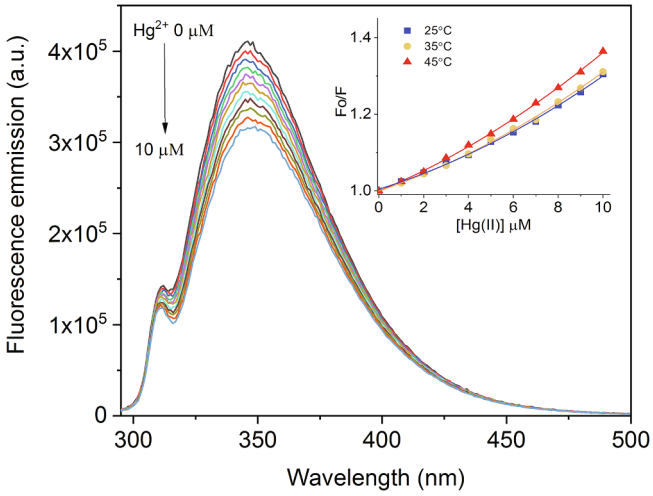

Fig. 8. Fluorescence spectra of 10 μM **Penta 3** following titration with increasing concentrations of mercury(II) at 20°C. Inset: Stern-Volmer plots at 25°C, 35°C, and 45°C.

Under the same experimental conditions, **Penta 3** show less significant fluorescence quenching (ca. 20%) following titrations with mercury(II) (Fig. 8). Stern-Volmer plots of the fluorescence emission spectra of **Penta 3** also show combined dynamic and static quenching characterized by an upward curvature, concave toward the y-axis. In contrast to **Penta 2**, it exhibits temperature dependent quenching at 45°C indicating that molecular contact between the indole ring and the quencher involves substantial collisional quenching at this temperature.

3.4. Computational studies

The binding activity of tryptophan side-chain group in a 1:1 mercury(II)-pentapeptide complexes was studied by analyzing complex structures of **Penta 1**, **Penta 2** and **Penta 3** using DFT and *ab initio* methods. Fig. 9 shows the structures with the lowest Gibbs energy in solution (G_{soln}) found for each of the three complexes. All pentapeptides are in a zwitterion protonation state and the thiol groups are deprotonated to bind with mercury(II), therefore all complexes are neutral. The molecular energies used to calculate Gibbs energy in solution (G_{soln}) for each complex in Fig. 9, and complexes found that are within 5 kJ/mol of the lowest energy structures (Fig. S2) are provided in Table S1. Higher energy complexes share the same root name appended with a, b or c from low to high energy, respectively. Coordinates and select Gaussian output information for all structures are specified in Table S2.

Stable complexes (Fig. 9) form having two S-Hg bonds with lengths of ~2.4 Å whereby a ring forms leaving the N- and C-terminal glycine amino acids external to the ring. The two bonds make S—Hg—S angles typically in the range of 175–178°. One C-terminal carboxylate oxygen forms a hydrogen bond with the *N*-terminal ammonium group with a NH—O distance of ~1.5 Å (Table 1). With the exception of **Penta 2**, both cysteine amide oxygen atoms have an O—Hg interaction. The typical O—Hg interaction distance is 2.65–2.75 Å for Cys-2 and 2.87 Å for Csy-4. Within **Penta 2**, a C-terminal carboxylate oxygen interacts with the coordinated mercury yielding a O—Hg distance of 2.825 Å and the Cys-2 carbonyl oxygen is rotated away from the mercury due to the presence of the tryptophan indole group.

Penta 1 serves as the reference due to the lack of a tryptophan side group. In addition to the structural features already described, the **Penta 1** complex includes two hydrogen-bonding interactions between amide N—H of both cysteines and the carboxylate oxygen that is not interacting with the *N*-terminal ammonium group. These are weaker than the hydrogen bond involving the ammonium group as indicated by the longer NH—O distances of 1.77 Å and 1.99 Å. If the amide group between Trp-3 and Cys-4 rotates upward, a hydrogen bond forms

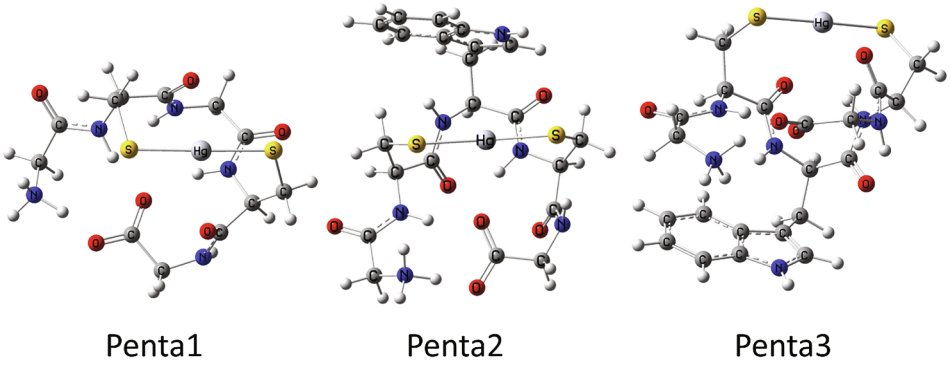

Fig. 9. Most stable structures found for each mercury(II) complex: **Penta 1**, **Penta 2** and **Penta 3**.

Table 1
Select geometric structural information for bonds and interactions of energy-minimized structures.

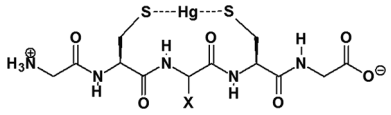

	Penta 1	Penta 2	Penta 3
Distance (Hg-S) (Å)	2.38	2.41	2.40/2.38
Angle S-Hg-S (deg)	177.9	156.4	175.0
Distance ammonium NH—O - C═O (Å)	1.51	1.47	1.52
Distance Hg—O═C (Å)			
Cys-2 carbonyl	2.87		2.87
Cys-4 carbonyl	2.75		2.65
C-terminal carboxylate		2.83	

between the Cys-4 NH and the Cys-2 amide oxygen, and also, the Trp-3 amide oxygen hydrogen bonds with the Gly-5 NH (**Penta 1a** in Fig. S2; NH—O = 2.22 Å and 2.15 Å, respectively). The Gibbs energy in solution for the **Penta 1a** complex is predicted to increase by 4.5 kJ/mol relative to **Penta 1**.

The peptide backbone of **Penta 3** (D-Trp) complex is similar to that of **Penta 1a**. The Cys-4 N—H hydrogen bond with the Cys-2 amide oxygen and the Trp-3 amide oxygen hydrogen bond with the Gly-5 N—H (NH—O = 2.17 Å and 2.15 Å, respectively). The tryptophan indole ring is oriented away from the S-Hg-S coordination site and is drawn close to the N-terminal ammonium group. In this ammonium-indole interaction, one of the ammonium hydrogens points toward the ring-fusing indole carbons, with H—C distances of 2.58 Å and 2.63 Å. Similar types of interactions (NH—pi) involving a cationic amino group and pi systems were previously characterized as a hydrogen bond (H-bond) due to their "intervening position" between the ammonium cation and the pi-electron center [42,43].

If the N-terminal ammonium group rotates up and away (via rotation of the amide C-Cα bond) from the indole to lose the cation-pi interaction, complex **Penta 3a** (Fig. S2) forms with a predicted increase in Gibbs energy of 2.2 kJ/mol. For a rotation of the ammonium group (via rotation of the ammonium N-Cα bond) while conserving the cation-pi interaction and shifting the ammonium to carboxylate hydrogen bond to the more inward carboxylate oxygen **Penta 3b** forms with a predicted increase in Gibbs energy of 4.7 kJ/mol relative to **Penta 3**.

The **Penta 2** (L-Trp) complex exhibits larger peptide backbone deviations from that of **Penta 1**. Its Cys-2 carbonyl is rotated to make room for the tryptophan indole ring to position its pi-system near the S-Hg-S coordination site in a mercury cation-pi interaction. The indole nitrogen and adjacent C-2 are closest to the coordinated mercury with distances of 3.60 Å and 3.56 Å, respectively. Similar preferences for the pyrrolo, rather than benzo subunit of the indole pi system has been reported by others for some alkali cation-pi interactions [44]. Its Cys-4 carbonyl also rotates away from the coordinated mercury and the carboxylate group replaces it with a new O—Hg interaction (2.8 Å). These interactions possibly cause the S-Hg-S angle to decrease by over 20 degrees relative to **Penta 1** (Table 1). A final feature of interest is the deviation from planarity of the amide bond between Trp-3 and Cys-4. The amide O—C—N—H dihedral angle is 150.4 degrees with the nitrogen directed toward the mercury atom giving an N—Hg distance of 2.93 Å. This decrease in dihedral angle also minimizes the Cys-4 NH to Cys-2 carbonyl oxygen distance (NH—O = 1.96 Å), which improves the hydrogen bonding interaction.

Penta 2a has the same peptide backbone structure as **Penta 1a** with the indole ring directed toward the Cys-4 thiolate of the mercury(II) coordination site (Fig. S2). **Penta 2a** is predicted to have a Gibbs energy greater than **Penta 2** by only 0.3 kJ/mol. If the indole ring rotates and is directed toward the Cys-2 thiolate side of the coordination site **Penta 2c** forms with a predicted Gibbs energy 4.8 kJ/mol greater than **Penta 2**. When only the indole ring is rotated in the **Penta 2** complex to yield **Penta 2b**, the mercury cation-pi interaction is closer to the benzo ring, instead of the pyrrolo ring, the Gibbs energy is predicted to increase by 3.0 kJ/mol relative to **Penta 2**.

4. Discussion

Bis-cysteinyl peptide sequences are well known in coordinating heavy metal ions due to favorable soft base/soft acid interactions [45–47]. Additionally, the propensity of tryptophan to participate in non-covalent pi-cation interactions is common and such associations play an important role in stabilizing the structure or contributing to the functional role of macromolecules in many biological systems [10–12]. From these established properties, we postulate that the indole ring could participate in auxiliary binding in thiolated mercury(II)-peptide complexes via cation-pi interactions and provide a hydrophobic barrier that shields the coordinated mercury ion. The difference absorption UV spectra of these pentapeptides show LMCT transition energy bands for the thiolated mercury(II) below 250 nm, which is consistent with the formation of bisthiolated mercury(II)-peptide complexes. Additionally, changes in the B_b absorption of the indole ring in **Penta 2** produced an absorption difference band with a maximum centered at 227 nm. This reflects a red-shift in the strong B_b transition of the indole ring from ca. 220 nm to 227 nm. Similar shifts are attributed to cation-pi interactions between the tryptophan indole ring and various types of cationic species, including imidazolium cation, K^+ and Cu^{2+} ions [37,48]. This suggests that the indole ring in **Penta 2** could be interacting with a cationic species, such as the coordinated mercury ion, N-terminal ammonium group, or other kinds of cations that are present. Previous work by others have shown that the weakening of the B_b absorption accompanied by a small red-shift is common for cation-pi interactions involving the indole ring, and that it is independent of cation type [49].

Some cation-pi interactions involving the indole ring also affect the

CD spectrum. This evidence was first reported for a cation-pi interaction between Cu^{2+} and tryptophan, which produced a negative band at 223 nm for neuromedin C in equimolar Cu^{2+}, and a model tetrapeptide representing the ATCUN motif on binding Cu^{2+} [37]. The CD spectra of **Penta 2** following titration with incremental mercury(II) develops a similar negative band at ca. 221 nm. This similarity in CD data and the red-shift of the B_b transition band of the indole ring for **Penta 2** provide complementary evidences that the indole ring in **Penta 2** is associating with the coordinated mercury(II) via a cation-pi interaction.

Penta 3 exhibits similar UV absorption difference spectra as observed for **Penta 2,** and it shows a comparable small red-shift in the B_b absorption of the indole ring. However, its CD spectra following titrations under analogous conditions for **Penta 2** did not produce a strong negative band at 221 nm. These data indicate that reversing the configuration for the tryptophan residue likely positioned the indole ring away from the coordinated mercury(II) for **Penta 3**. Nonetheless, the indole ring is interacting with a cationic species resulting in changes of its B_b absorption. To investigate these findings further, changes in the intrinsic fluorescence of **Penta 2** and **Penta 3** were compared following titrations with mercury(II).

Penta 2 exhibits stronger fluorescence quenching (more than three times) at equimolar ratio of mercury(II) to peptide than **Penta 3**. This is indicative of an association between its indole ring and mercury(II) because the latter is a strong fluorescence quencher. Stern-Volmer plots also show that **Penta 2** exhibits considerable static quenching due to complex formation and some degree of collisional quenching due to diffusion. These results are consistent with the corresponding UV and CD data for **Penta 2**, and indicate that the tryptophan indole ring is associating with the thiolated mercury(II). In contrast, the intrinsic fluorescence of **Penta 3** is quenched by only about 20% in equimolar mercury(II) and it demonstrates more substantial collisional quenching than that observed for **Penta 2**. Although **Penta 3** displays similar UV results as **Penta 2**, its CD spectral data do not indicate strong mercury (II) cation-pi interaction. These comparative spectroscopic results show that the mode of fluorescence quenching in **Penta 2** and **Penta 3** is different and likely arise from the association of their respective indole group with two different types of quencher, which also affect changes to the B_b absorption of the indole ring. The fluorescence of the tryptophan indole ring is very sensitive to its environment and it can be quenched by interaction with amide, ammonium, carboxylate, or other electron-acceptor quenching groups that are in proximity [11,39,50–52].

The geometry optimized structures for the pentapeptide-mercury(II) complexes provided further insights into possible types of interaction involving the indole ring. In the predicted lowest free energy structure for the 1:1 mercury(II)-**Penta 2** complex, the tryptophan indole ring is oriented close to the mercury(II) coordination site to be involved in a mercury(II) cation-pi interaction. This is in agreement with the spectroscopic characteristics reported in the results section. Other optimized conformations for this complex that are within 5 kJ/mol of the most stable structure show some variations in which the hydrophobic indole ring could shield the coordination site. One of these higher energy structures has a similar binding motif as **Penta 2**. In contrast, the lowest free energy structure for the 1:1 mercury(II)-**Penta 3** complex reveals that the D-tryptophan indole ring is not close to the mercury(II) coordination site, which is in agreement with its CD spectral characteristics and weaker fluorescence quenching. Instead, it is positioned close to the *N*-terminal ammonium group and maintains an ammonium cation-pi (NH-pi) interaction. This interaction could account for the observed changes in the indole B_b absorption band in the UV region. The orientation of the D-tryptophan indole ring away from the coordination site is consistent among the three lowest energy structures for this complex.

The main difference between the optimized structures for **Penta 2** and **Penta 3** complexes is the orientation of the tryptophan indole ring. The coordination geometry in the lowest free energy structure for the **Penta 2** complex involves placement of its indole ring close to the mercury(II) coordination site. This is accompanied by the bending of the S-Hg-S unit, conceivably caused by the interaction of the coordinated mercury(II) with the carboxylate oxygen (O—Hg) and the amide nitrogen (N—Hg) donor groups. In addition, the peptide backbone deviates somewhat from that adopted by **Penta 1** and **Penta 3** mercury complexes, possibly to enable the orientation of the indole ring to interact with the coordinated mercury(II). It is noteworthy that the **Penta 2** complex accommodates these geometric deviations to facilitate auxiliary binding of mercury by the indole ring. As previously reported by others, metal cation-pi interaction is an important non-covalent bonding that provides significant stabilization [10–12, 53,54]. Therefore, it is likely to have a profound influence in regulating its structural environment.

5. Conclusion

In this study, we investigated the possible involvement of the indole side chain of tryptophan in potential auxiliary binding within thiolated mercury(II) pentapeptides. By combining some spectroscopic and theoretical studies, we have gained important structural insights into how these model peptides coordinate mercury(II). They bind mercury(II) by forming 1:1 bisthiolated mercury(II) complexes whereby the peptide backbone adopts a reverse turn that resembles the type I β turn peptide structure. Some structural changes in the peptide backbone enable the tryptophan indole ring in **Penta 2** to associate with the bisthiolated mercury(II) at the coordination site via cation-pi interaction. This cooperative binding feature shows that the indole ring of tryptophan can participate in auxiliary binding of mercury(II) and provide a hydrophobic shielding of the coordination site. This could prevent the complexed mercury ion from undergoing exchange with other competing ligands. Such inert mercury(II) complexes could enhance the immobilization of mercury and it may prove advantageous for the development of better chelators for mercury ions. The Cys-Trp-Cys mercury(II) binding motif may be useful for the development of chelators for effective immobilization of mercury(II).

CRediT authorship contribution statement

Maria Ngu-Schwemlein: Conceptualization, Methodology, Validation, Investigation, Resources, Writing - original draft, Visualization, Supervision, Funding acquisition, Writing - review & editing. **John Merle:** Investigation, Resources, Funding acquisition, Writing - original draft. **William Meeker:** Investigation. **Kierah Risdon-Langdon:** Investigation. **Timothy Nixon:** Investigation.

Declaration of Competing Interest

The authors declare that they have no known competing financial interests or personal relationships that could have appeared to influence the work reported in this paper.

Acknowledgements

This work was supported by the National Science Foundation grant CHE-1831020.

Appendix A. Supplementary data

Supplementary data to this article can be found online at https://doi.org/10.1016/j.ica.2020.119552.

References

[1] R.A. Steele, S.J. Opella, Structures of the reduced and mercury-bound forms of MerP, the periplasmic protein from the bacterial mercury detoxification system, Biochemistry 36 (23) (1997) 6885–6895.

[2] P. Lian, H.-B. Guo, D. Riccardi, A. Dong, J.M. Parks, Q. Xu, E.F. Pai, S.M. Miller, D.-Q. Wei, J.C. Smith, H. Guo, X-ray structure of a Hg^{2+} complex of mercuric reductase (MerA) and quantum mechanical/molecular mechanical study of Hg^{2+} transfer between the C-terminal and buried catalytic site cysteine pairs, Biochemistry 53 (46) (2014) 7211–7222.

[3] N.L. Brown, Bacterial resistance to mercury — reductio ad absurdum? Trends Biochem. Sci. 10 (10) (1985) 400–403.

[4] F. Tatsuhiko, K. Masaharu, I. Ryuji, T. Kazutake, A. Shin-ichi, Copper transport systems are involved in multidrug resistance and drug transport, Curr. Med. Chem. 15 (30) (2008) 3268–3278.

[5] F. Hussain, P. Wittung-Stafshede, Impact of cofactor on stability of bacterial (CopZ) and human (Atox1) copper chaperones, Biochim. Biophys. Acta, Proteins Proteomics 1774 (10) (2007) 1316–1322.

[6] S. Pires, J. Habjanič, M. Sezer, C.M. Soares, L. Hemmingsen, O. Iranzo, Design of a peptidic turn with high affinity for Hg(II), Inorg. Chem. 51 (21) (2012) 11339–11348.

[7] K. Kulon, D. Wozniak, K. Wegner, Z. Grzonka, H. Kozlowski, Specific interactions of metal ions with Cys-Xaa-Cys unit inserted into the peptide sequence, J. Inorg. Biochem. 101 (11–12) (2007) 1699–1706.

[8] P. Rousselot-Pailley, O. Sénèque, C. Lebrun, S. Crouzy, D. Boturyn, P. Dumy, M. Ferrand, P. Delangle, Model peptides based on the binding loop of the copper metallochaperone Atx1: selectivity of the consensus sequence MxCxxC for metal ions Hg(II), Cu(I), Cd(II), Pb(II), and Zn(II), Inorg. Chem. 45 (14) (2006) 5510–5520.

[9] D.A. Dougherty, Cation-pi interactions in chemistry and biology: a new view of benzene, Phe, Tyr, and Trp, Science 271 (5246) (1996) 163–168.

[10] J.C. Ma, D.A. Dougherty, The cation-pi interaction, Chem. Rev. 97 (5) (1997) 1303–1324.

[11] D.A. Dougherty, The cation–π interaction, Acc. Chem. Res. 46 (4) (2013) 885–893.

[12] A.S. Mahadevi, G.N. Sastry, Cation-pi interaction: its role and relevance in chemistry, biology, and material science, Chem. Rev. 113 (3) (2013) 2100–2138.

[13] D.K. Chakravorty, B. Wang, M.N. Ucisik, K.M. Merz Jr., Insight into the cation-pi interaction at the metal binding site of the copper metallochaperone CusF, J. Am. Chem. Soc. 133 (48) (2011) 19330–19333.

[14] S. Medici, M. Peana, V.M. Nurchi, M.A. Zoroddu, The involvement of amino acid side chains in shielding the nickel coordination site: an NMR study, Molecules 18 (10) (2013) 12396–12414.

[15] T.W. Craven, M.K. Cho, N.J. Traaseth, R. Bonneau, K. Kirshenbaum, A miniature protein stabilized by a cation-pi interaction network, J. Am. Chem. Soc. 138 (5) (2016) 1543–1550.

[16] T. Kamiyama, T. Miura, H. Takeuchi, His-Trp cation-pi interaction and its structural role in an alpha-helical dimer of HIV-1 Vpr protein, Biophys. Chem. 173–174 (2013) 8–14.

[17] R.M. Hughes, M.L. Waters, Arginine methylation in a beta-hairpin peptide: implications for Arg-pi interactions, DeltaCp(o), and the cold denatured state, J. Am. Chem. Soc. 128 (39) (2006) 12735–12742.

[18] M.M. Yamashita, L. Wesson, G. Eisenman, D. Eisenberg, Where metal ions bind in proteins, Proc. Natl. Acad. Sci. U.S.A. 87 (15) (1990) 5648–5652.

[19] W. Bal, G.N. Chmurny, B.D. Hilton, P.J. Sadler, A. Tucker, axial hydrophobic fence in highly-stable Ni(II) complex of des-angiotensinogen N-terminal peptide, J. Am. Chem. Soc. 118 (19) (1996) 4727–4728.

[20] S.D. Zaric, D.M. Popovic, E.W. Knapp, Metal ligand aromatic cation-pi interactions in metalloproteins: ligands coordinated to metal interact with aromatic residues, Chemistry 6 (21) (2000) 3935–3942.

[21] J. Merle, J. Mazlo, J. Watts, R. Moreno, M. Ngu-Schwemlein, Reaction mixture analysis by ESI-MS: mercury(II) and dicysteinyl tripeptide complex formation, Int. J. Mass Spectrom. 426 (2018) 38–47.

[22] B.J. Kuipers, H. Gruppen, Prediction of molar extinction coefficients of proteins and peptides using UV absorption of the constituent amino acids at 214 nm to enable quantitative reverse phase high-performance liquid chromatography-mass spectrometry analysis, J. Agric. Food Chem. 55 (14) (2007) 5445–5451.

[23] J.R. Lakowicz, Principles of Fluorescence Spectroscopy, 3rd ed., Springer Science and Business Media, LLC, New York, 2006, pp. 278–318.

[24] MacroModel, Release 2019-1; Schrödinger, LLC: New York, 2019.

[25] D. Andrae, U. Häußermann, M. Dolg, H. Stoll, H. Preuß, Energy-adjustedab initio pseudopotentials for the second and third row transition elements, Theor. Chim. Acta 77 (2) (1990) 123–141.

[26] H. Valdes, K. Pluhackova, M. Pitonak, J. Rezac, P. Hobza, Benchmark database on isolated small peptides containing an aromatic side chain: comparison between wave function and density functional theory methods and empirical force field, Phys. Chem. Chem. Phys. 10 (19) (2008) 2747–2757.

[27] J. Watts, E. Howell, J.K. Merle, Theoretical studies of complexes between Hg(II) ions and l-cysteinate amino acids, Int. J. Quantum Chem. 114 (5) (2014) 333–339.

[28] A.V. Marenich, C.J. Cramer, D.G. Truhlar, Universal solvation model based on solute electron density and on a continuum model of the solvent defined by the bulk dielectric constant and atomic surface tensions, J. Phys. Chem. B 113 (18) (2009) 6378–6396.

[29] R.F. Ribeiro, A.V. Marenich, C.J. Cramer, D.G. Truhlar, Use of solution-phase vibrational frequencies in continuum models for the free energy of solvation, J. Phys. Chem. B 115 (49) (2011) 14556–14562.

[30] Johnson III, R. D. NIST Computational Chemistry Comparison and Benchmark Database NIST Standard Reference Database Number 101 Release 20, 2019.

[31] M.J. Frisch, G.W. Trucks, H.B. Schlegel, G.E. Scuseria, M.A. Robb, J.R. Cheeseman, et al., Gaussian 09, Revision C.01, Gaussian, Inc., Wallingford CT, 2009.

[32] O. Iranzo, P.W. Thulstrup, S.-B. Ryu, L. Hemmingsen, V.L. Pecoraro, The application of 199Hg NMR and 199mHg perturbed angular correlation (PAC) spectroscopy to define the biological chemistry of Hg(II): a case study with designed two- and three-stranded coiled coils, Chem. Eur. J. 13 (33) (2007) 9178–9190.

[33] O. Iranzo, D. Ghosh, V.L. Pecoraro, Assessing the integrity of designed homomeric parallel three-stranded coiled coils in the presence of metal ions, Inorg. Chem. 45 (25) (2006) 9959–9973.

[34] M. Łuczkowski, M. Stachura, V. Schirf, B. Demeler, L. Hemmingsen, V.L. Pecoraro, Design of thiolate rich metal binding sites within a peptidic framework, Inorg. Chem. 47 (23) (2008) 10875–10888.

[35] M. Matzapetakis, B.T. Farrer, T.-C. Weng, L. Hemmingsen, J.E. Penner-Hahn, V.L. Pecoraro, Comparison of the binding of cadmium(II), mercury(II), and arsenic (III) to the de novo designed peptides TRI L12C and TRI L16C, J. Am. Chem. Soc. 124 (27) (2002) 8042–8054.

[36] A. Perczel, M. Hollosi, Turns. In Circular Dichroism and the Conformational Analysis of Biomolecules, Fasman, G. D., Ed. Plenum: 1996; pp 285-380.

[37] H. Yorita, K. Otomo, H. Hiramatsu, A. Toyama, T. Miura, H. Takeuchi, Evidence for the cation-pi interaction between Cu^{2+} and tryptophan, J. Am. Chem. Soc. 130 (46) (2008) 15266–15267.

[38] R.W. Woody, Theory of Circular Dichroism of Proteins. In Circular Dichroism and the Conformational Analysis of Biomolecules, Fasman, G. D., Ed. Plenum: 1996; pp. 25–67.

[39] J.R. Lakowicz, Principles of Fluorescence Spectroscopy, 3rd ed., Springer Science and Business Media, LLC, New York, 2006, pp. 529–567.

[40] L.J. Juszczak, A.S. Eisenberg, The color of cation-pi interactions: subtleties of amine-tryptophan interaction energetics allow for radical-like visible absorbance and fluorescence, J. Am. Chem. Soc. 139 (24) (2017) 8302–8311.

[41] E.A. Orabi, G. Lamoureux, Cation–π interactions between quaternary ammonium ions and amino acid aromatic groups in aqueous solution, J. Phys. Chem. B 122 (8) (2018) 2251–2260.

[42] H. Basch, W.J. Stevens, Hydrogen bonding between aromatics and cationic amino groups, J. Mol. Struct.: Theochem. 338 (1) (1995) 303–315.

[43] C.H. Gorbitz, L.M. Hartviksen, The monohydrates of the four polar dipeptides l-seryl-l-asparagine, l-seryl-l-tyrosine, l-tryptophanyl-l-serine and l-tyrosyl-l-tryptophan, Acta Crystallogr., Sect. C: Struct. Chem. 64 (3) (2008) o171–o176.

[44] S.L. De Wall, E.S. Meadows, L.J. Barbour, G.W. Gokel, Solution- and solid-state evidence for alkali metal cation–π interactions with indole, the side chain of tryptophan, J. Am. Chem. Soc. 121 (23) (1999) 5613–5614.

[45] R.G. Pearson, Hard and soft acids and bases, J. Am. Chem. Soc. 85 (22) (1963) 3533–3539.

[46] J.E. Huheey, E.A. Keiter, R.L. Keiter, Inorganic Chemistry: Principles of Structure and Reactivity, fourth ed., Harper Collins College Publishers, New York, 1993.

[47] X. Lin, J. Brooks, M. Bronson, M. Ngu-Schwemlein, Evaluation of the association of mercury(II) with some dicysteinyl tripeptides, Bioorg. Chem. 44 (2012) 8–18.

[48] A. Okada, T. Miura, H. Takeuchi, Protonation of histidine and histidine–tryptophan interaction in the activation of the M2 ion channel from influenza A virus, Biochemistry 40 (20) (2001) 6053–6060.

[49] Y. Xue, A.V. Davis, G. Balakrishnan, J.P. Stasser, B.M. Staehlin, P. Focia, T.G. Spiro, J.E. Penner-Hahn, T.V. O'Halloran, Cu(I) recognition via cation-π and methionine interactions in CusF, Nat. Chem. Biol. 4 (2) (2008) 107–109.

[50] R.W. Alston, M. Lasagna, G.R. Grimsley, J.M. Scholtz, G.D. Reinhart, C.N. Pace, Peptide sequence and conformation strongly influence tryptophan fluorescence, Biophys. J. 94 (6) (2008) 2280–2287.

[51] Y. Chen, M.D. Barkley, Toward understanding tryptophan fluorescence in proteins, Biochemistry 37 (28) (1998) 9976–9982.

[52] Y. Chen, B. Liu, H.-T. Yu, M.D. Barkley, The peptide bond quenches indole fluorescence, J. Am. Chem. Soc. 118 (39) (1996) 9271–9278.

[53] Ç.A. Demircan, U. Bozkaya, Transition metal cation–π interactions: complexes formed by Fe^{2+}, Co^{2+}, Ni^{2+}, Cu^{2+}, and Zn^{2+} binding with benzene molecules, J. Phys. Chem. A 121 (34) (2017) 6500–6509.

[54] S. Kolakkandy, S. Pratihar, A.J.A. Aquino, H. Wang, W.L. Hase, Properties of complexes formed by Na^{+}, Mg^{2+}, and Fe^{2+} binding with benzene molecules, J. Phys. Chem. A 118 (40) (2014) 9500–9511.